Mitotic gene bookmarking by RUNX1 contributes to stabilization of the normal mammary epithelial phenotype

Joshua T. Rose[1], Joseph R. Boyd[1], Jonathan A. Gordon[1], Mingu Kang[1], Eliana Moskovitz[1], Nicole A. Bouffard[2], Andrew J. Fritz[1], Anuradha Illendula[3], John H. Bushweller[3], Jane B. Lian[1], Janet L. Stein[1], Gary S. Stein[1], and Sayyed K. Zaidi[1*]

[1]Department of Biochemistry and University of Vermont Cancer Center, Robert Larner College of Medicine, 89 Beaumont Avenue, Burlington, VT 05405, USA

[2]Microscopy Imaging Center at the Robert Larner College of Medicine, 89 Beaumont Avenue, Burlington, VT 05405, USA

[3]Department of Molecular Physiology and Biological Physics, University of Virginia, Charlottesville, VA 22908, USA

*Corresponding Author

Sayyed K Zaidi, PhD

sayyed.zaidi@med.uvm.edu

Room E210, Given Building

University of Vermont

89 Beaumont Avenue, Burlington VT 05405

Key Words: Mammary phenotype, epithelial phenotype, RUNX1, mitotic gene bookmarking.

Summary Statement

This study elucidates mitotic gene bookmarking as a novel epigenetic mechanism in breast epithelial cells which impacts cell growth and phenotype and has potential implications in breast cancer onset.

Abstract

Loss of the RUNX1 transcription factor leads to epithelial-to-mesenchymal transition (EMT), but mechanisms by which RUNX1 stabilizes the mammary epithelial phenotype are not known. Here, we report RUNX1 gene bookmarking during mitosis as one of the key epigenetic mechanisms to convey regulatory information for coordinate control of mammary cell proliferation, growth, and identity through successive cell divisions. Genome-wide RUNX1 occupancy profiles for asynchronous, mitotically-enriched, and G1 breast epithelial cells reveal RUNX1 is retained during mitosis on RNA Pol I- (i.e., ribosomal RNA) and II-transcribed protein coding (e.g., *HES1*) and long non-coding RNA (e.g., *NEAT1*) genes controlling proliferation, growth, and mammary epithelial phenotype maintenance. Disruption of RUNX1 DNA binding and target gene occupancy alters cell morphology, global protein synthesis, and phenotype-related gene expression. Together, these findings demonstrate that RUNX1 mitotic bookmarking contributes to maintenance of the normal mammary epithelial phenotype. Compromising RUNX1 DNA binding initiates EMT, an essential first step in the onset of breast cancer.

Breast cancer arises from a series of acquired mutations and epigenetic changes that disrupt normal mammary epithelial homeostasis and create multi-potent cells that can differentiate into biologically unique clinically distinct subtypes. Epithelial-to-mesenchymal transition (EMT) – a trans-differentiation process through which mammary epithelial cells acquire an aggressive mesenchymal phenotype – is a key driver of breast cancer progression, invasion and metastasis [1]. Transcription factors Snail, Slug, Twist, and Zeb1/2 contribute to EMT during early, normal development and have also been implicated in invasion [2-5]. Despite accumulating evidence for a broad understanding of EMT regulation and maintenance of the epithelial phenotype, the mechanism(s) by which mammary epithelial cells maintain their biological phenotype is unknown.

Runt-Related Transcription Factor 1 (RUNX1/AML1) is required for hematopoietic lineage specification during development and hematopoiesis throughout life [6-19]. In addition to the recognized role in hematological malignancies, RUNX1 has been recently identified as a key player in breast cancer development and tumor progression [20-24]. RUNX1 is significantly mutated in breast tumors [25-27]. Findings from our group, reinforced by studies from others, have shown that RUNX1 maintains breast epithelial phenotype and prevents EMT through transcriptional regulation of genes involved in key cellular pathways [23]. This regulation is reflected by RUNX1 control of E-cadherin expression, a key cell adhesion protein and marker of EMT [28]. Consequently, there is a requirement to understand epigenetic mechanisms by which RUNX1 stabilizes the normal mammary epithelial phenotype.

Mitotic gene bookmarking, i.e. transcription factor binding to target genes during mitosis for transcriptional regulation following cell division, is a key epigenetic mechanism

to convey and sustain regulatory information for cell proliferation, growth, and cell identity from parent to progeny cells [29-31]. Phenotypic transcription factors that include GATA1, RBPJ, FoxA1, SOX2, OCT4, and KLF4, bookmark target genes during mitosis [32-36]. We have established that RUNX proteins as well as other phenotypic transcription factors that include MYOD and CEBPα bookmark RNA Pol I- and II-transcribed genes during mitosis for coordinate control of cell growth, proliferation and phenotype. [37-40]

We addressed the hypothesis that RUNX1 maintains the breast epithelial phenotype by mitotic bookmarking of genes that support mammary epithelial proliferation, growth, and phenotype during mitosis for expression immediately after cell division. Immunofluorescence confocal microscopy revealed that RUNX1 is present on chromosomes throughout mitosis and colocalizes with upstream binding transcription factor (UBF), a subunit of RNA Pol I transcriptional machinery. To identify genes occupied by RUNX1, we performed chromatin immunoprecipitation coupled with high throughput sequencing (ChIP-Seq) using a RUNX1-specific antibody on mitotic, G1, and asynchronous normal mammary epithelial MCF10A cells. ChIP-Seq revealed that, in mitosis, RUNX1 associates with RNA Pol II regulated genes specifically involved in maintenance of the epithelial phenotype and EMT progression. Interestingly, ribosomal RNA genes, regulated by the RNA Pol I transcriptional machinery, were occupied by RUNX1. A fluorescence-based, global protein synthesis assay showed reduced protein synthesis when RUNX1 DNA binding was perturbed using a small molecule inhibitor. Strikingly, inhibition of RUNX1 resulted in loss of the epithelial phenotype and acquisition of mesenchymal properties. These findings establish mitotic gene bookmarking as a key mechanism for RUNX1 stabilization of the normal breast epithelial phenotype.

Importantly, disruption of RUNX1 mitotic bookmarking initiates EMT, an early event in the onset of breast cancer.

RESULTS

RUNX1 associates with mitotic chromatin and occupies target genes

To investigate subcellular localization of RUNX1 in normal mammary epithelial cells, we performed immunofluorescence microscopy in actively proliferating MCF10A cells. We observed that RUNX1 is distributed in punctate subnuclear domains throughout interphase nuclei (Fig. 1; the Interphase panel). Interestingly, RUNX1 is localized on mitotic chromatin at all topologically identified substages of mitosis (Fig 1; top panels). Two distinct types of foci are detectable on mitotic chromosomes: 2-8 large punctate foci that appear to be allelic as well as numerous smaller foci that were distributed across the chromosomes (Fig 1; bottom panels, white arrowheads). In agreement with our previous findings, RUNX1 foci are equally distributed into resulting progeny cells [40]. Presence of RUNX1 at all stages of mitosis indicates that the protein is stable during cell division.

To experimentally address RUNX1 occupancy of target genes, MCF10A cells were synchronized in mitosis using nocodazole (50ng/mL); additionally, cells in the G1 cell cycle stage was collected following a 3hr release from the block (Fig. 2A). Mitotic purity of harvested cells was confirmed by the presence of H3pS28 (>99%; data not shown). Western blot analysis of whole cell lysates from the three cell populations show expected levels of expression for cell cycle-specific proteins Cyclin B and CDT1 (Fig. 2B). FACS profiles of cell populations confirmed the characteristic enrichment of blocked cells in mitosis (Fig 2C; Mitotic) and release into G1 upon media replacement (Fig 1C; G1) when

compared to asynchronous cells (Fig 2C; Asynch). Consistent with immunofluorescence observations, RUNX1 was present in all three cell populations (Supplement Fig. 1). Together, these results demonstrate that RUNX1 is stable through mitosis and localizes to mitotic chromatin.

We next determined if RUNX1 remains bound to target genes during mitosis, ChIP-Seq was performed on Asynch, Mitotic, and G1 MCF10A cells using a RUNX1 specific antibody (Fig. 2D). Sequencing datasets were mapped to the latest human genome build (hg38) using Bowtie2. Enriched regions were determined using Model-Based Analysis of ChIP-Seq (MACS) and were analyzed at $p<10^{-5}$ significance level with an irreproducible discovery rate (IDR) of 0.05. Heatmaps of RUNX1-occupied genes in all three cell populations were generated by seqsetvis (Bioconductor) (Fig 2D). Comparison of the three cell populations revealed subsets of genes that were either shared (354 genes) across the three groups or were specific for each, indicating dynamic binding of RUNX1 during and immediately after mitosis (Fig 2D). Peak calling identified RUNX1 occupancy of both protein coding and long non-coding RNA (lncRNA) genes. Specifically, RUNX1 occupied 2020 genes in Asynch population (Fig 2D; green bar) and 1095 genes G1-enriched cells (Fig 2D; light brown bar). Importantly, RUNX1 occupied 551 genes (413 protein coding and 138 lncRNAs) in mitotically-enriched MCF10A cells (Fig 2D; blue bar).

Functional relevance of RUNX1 occupancy in the three cell populations was determined by comparing RUNX1-occupied genes with those that are differentially regulated upon shRNA-mediated RUNX1 knockdown[23]. Critically important to our central hypothesis that RUNX1 mitotically bookmarks genes for regulation immediately after cell division and as shown in Fig 2D, 399 of 1268 RUNX1-bookmarked genes in the M and

G1 populations were deregulated upon RUNX1 depletion. These findings reveal that several hundred target genes are bookmarked by RUNX1 during mitosis and transcriptionally regulated in normal mammary epithelial cells. To identify cellular processes and pathways that comprise of RUNX1-bookmarked genes, we performed gene set enrichment analysis (GSEA) on genes bound by RUNX1 during mitosis or G1, or not bound in either cell cycle stage (Fig 2E). Interestingly, most genes bookmarked by RUNX1 during mitosis were associated with negative regulation of gene expression and metabolic process (Fig 2E; blue box). Consistent with cellular requirement to reattach and enter the next cell cycle and fully resume transcription, genes bound during G1 were primarily enriched in biological processes involving cell anchorage, protein localization and positive regulation of gene expression (Fig 2E; brown box). ChIP-seq results were further validated by motif analysis of RUNX1-bound peaks, which showed that RUNX motif was the top enriched motif in all three cell populations (Fig 2F). Importantly, RUNX1-bound genomic regions were also enriched in motifs for transcription factors known to cooperate with RUNX1 for gene regulation[41] (Fig 2F). Together, these findings indicate that RUNX1 bookmarks genes involved in cell proliferation, growth, and phenotype in normal mammary epithelial cells.

RUNX1 mitotically bookmarks RNA Pol I-transcribed genes that control cell growth

Our ChIP-Seq results revealed that RUNX1 occupies rDNA repeats in MCF10A mammary epithelial cells; all three MCF10A cell populations (Asynch, Mitotic and G1) exhibited significant fold enrichment within the promoter region of hrDNA (Fig 4A), suggesting a potential role for RUNX1 in regulating rRNA genes in MCF10A cells. We

157 confirmed this finding in actively proliferating MCF10A cells by immunofluorescence
158 microscopy for antibodies specific against RUNX1 and upstream binding factor (UBF), a
159 transcriptional activator that remains bound to rRNA genes during mitosis. We observed
160 large RUNX1 foci colocalizing with UBF throughout each stage of mitosis (Fig 3A; bottom
161 panels). Colocalization between RUNX1 and UBF was validated by confocal microscopy.
162 Line scans of MCF10A cells show that although RUNX1 and UBF occupy distinct nuclear
163 microenvironments in interphase (n=15), both proteins substantially colocalize in
164 metaphase (n=15) (Fig 3B). Taken together, these findings establish RUNX1 binding to
165 ribosomal DNA repeat regions identified by ChIP-Seq (Fig 4A) and confirmed at the
166 cellular level by confocal microscopy (Fig 3).

167 We experimentally addressed the hypothesis that RUNX1 regulates ribosomal
168 gene expression by using a pharmacological inhibitor of RUNX1. The small molecule
169 inhibitor—AI-14-91—interferes with RUNX1-CBFβ interaction and disrupts RUNX1 DNA
170 binding [42,43]. We first determined the effect of RUNX1 inhibitor on mitotic retention of the
171 protein. Actively proliferating MCF10A cells were treated with the inhibitor (AI-14-91) for
172 6hr, 12hr, 24hr, and 48hr at 20μM; a structurally equivalent inert compound (AI-4-88) was
173 used as a control under identical conditions. Cells were subjected to immunofluorescence
174 microscopy followed by detection of RUNX1 and UBF as described above. Although
175 RUNX1 signal was detected in all mitotic sub-stages (data not shown), we observed a
176 substantial decrease in RUNX1 signal intensity on mitotic chromosomes (white arrows;
177 Fig 4B), indicating that RUNX1-Cbfβ interaction and RUNX1 DNA binding activity plays a
178 key role in mitotic gene bookmarking. These changes were more pronounced for smaller
179 RUNX1 foci and were not observed in control-treated cells; appreciable signal for large

RUNX1 foci that colocalize with UBF (Fig 3) remained detectable in all sub-stages of mitosis (Fig 4B and data not shown).

We next examined the effect of RUNX1 inhibitor on pre-rRNA expression and found that pre-rRNA expression was significantly increased at 12hr and 48hr timepoints after treatment of asynchronous cells with specific RUNX1 inhibitor but not inactive compound, indicating that RUNX1 suppresses rRNA gene expression in normal mammary epithelial cells (Fig 4C). Because levels of rRNA directly correlate with global protein synthesis, a fluorescent-based detection method was used to measure newly synthesized proteins. Cells treated with AI-14-91 for 24hr or 48hr showed a moderate change in levels of global protein synthesis in comparison to control-treated cells under identical conditions (Fig 4D). Together, our results demonstrate that RUNX1 bookmarks RNA Pol I regulated rRNA genes during mitosis and transcriptionally represses them with moderate impact on global protein synthesis in normal mammary epithelial cells.

RUNX1 mitotically bookmarks RNA Pol II-transcribed genes involved in hormone-responsiveness and cell phenotype

Using RUNX1-bookmarked genes, gene set enrichment analysis (GSEA) was performed to identify regulatory pathways (Fig 5A). In agreement with known roles of RUNX1 [44-48], top 10 pathways identified were those involved in regulation of G2M Checkpoint, E2F targets, p53, and DNA repair (Fig 5A). Consistent with our finding that RUNX1 bookmarked and regulates rRNA genes, one of the pathways identified is mTOR signaling, a pathway that is required for cell growth and is a therapeutic target in breast cancers [49,50]. Relevant to the normal mammary epithelial phenotype, both early and late

estrogen response signaling gene sets significantly overlap with RUNX1 mitotically bookmarked genes (Fig 5A). Because estrogen plays vital roles in promoting proliferative phenotypes of mammary epithelial cells [51-53], we interrogated RUNX1 bookmarked genes to identify those bound by RUNX1 and ERα (Fig 5B) [54]. Using publicly available datasets of ERα genome-wide occupancy and estradiol-regulated gene expression, we find that a subset of genes mitotically bookmarked by RUNX1 is also bound by ERα, and either up or down regulated in response to estradiol. These findings indicate that RUNX1-bookmarked genes are involved in pathways that control hormone-responsiveness, proliferation and growth of normal mammary epithelial cells (Fig 5B).

A subset of RUNX1-bookmarked genes relates to regulatory pathways involved in cellular phenotype including TNFα, Apical Junction and Notch signaling (Fig 5A). Furthermore, NEAT1 and MALAT1, lncRNAs often deregulated in breast cancer [55,56], were also mitotically bookmarked by RUNX1. Of the 413 RUNX1 bookmarked protein coding genes, *TOP2A*, *MYC*, *HES1*, *RRAS*, *H2AFX*, and *CCND3* are representative of RNA Pol II-transcribed genes involved in phenotype maintenance and cell fate decisions (See Supplemental Table 1 for complete list). Recently, *HES1* and *H2AFX* have been identified as regulators of breast epithelial phenotype [57-59]. In our ChIP-seq dataset, *HES1* and *H2AFX* show significant fold enrichment of RUNX1 occupancy between the three populations of MCF10A cells (Fig 5C; top panels). Expression of *HES1* increased upon inhibition of RUNX1 DNA binding (Fig 5C; left panel—bar graph), indicating that RUNX1 represses *HES1*. In contrast, *H2AFX* expression at 24hr and 48hr of inhibitor treatment was decreased, suggesting RUNX1 activates H2AFX expression (Fig 5C; right panel—bar graph). These results indicate that by bookmarking both protein coding and non-

coding genes that are critical determinants of lineage identity, RUNX1 stabilizes the mammary epithelial phenotype.

Inhibition of RUNX1 DNA binding causes epithelial to mesenchymal transition

To experimentally address whether disruption of RUNX1 bookmarking leads to a change in epithelial phenotype, we treated cells with RUNX1 DNA binding inhibitor and monitored changes in cell morphology (Fig 6). Consistent with RUNX1 bookmarking and regulation of genes critical for epithelial phenotype (Fig 5), disruption of RUNX1 DNA binding resulted in mesenchymal morphology. We next examined whether long-term inhibition of RUNX1 caused a permanent change in cell phenotype. Longer term treatment (5 days) of actively proliferating MCF10A cells showed significant apoptosis, although a small sub-population of cells survived and exhibited an altered phenotype (Fig 6B). The surviving sub-population at day 5 was recovered by culturing cells in media without the inhibitor. By day 3-4 following media replacement, cells clearly showed a mesenchymal morphology (Fig 6B), indicating that interfering with RUNX1 mitotic bookmarking causes loss of the normal mammary epithelial phenotype. Consistent with changes in cell morphology, we find alterations in expression and localization of the cytoskeletal F-actin protein (Fig 6C). These observations were confirmed by examining the expression of epithelial markers (e.g., E Cadherin (Fig 6D)), as well as mesenchymal markers (e.g., SNAI2 (Fig 6E)). E-cadherin was partially downregulated, while SNAI2 expression was significantly increased, confirming an epithelial-to-mesenchymal transition upon inhibition of the RUNX1-Cbfβ interaction. The p21 gene, a known target that is repressed by RUNX1, was included as a control and, as expected, showed an

249 increased expression with the inhibitor treatment (Fig 6E; right panel). Together, these
250 findings show that RUNX1 mitotic bookmarking of epithelial cell growth, proliferation, and
251 lineage-related genes is a key epigenetic mechanism required to stabilize the normal
252 mammary epithelial phenotype. Disruption of RUNX1 gene bookmarking results in an
253 epithelial-to-mesenchymal transition, a key first event at the onset of breast cancer.

DISCUSSION

This study identifies RUNX1 mitotic bookmarking as a novel epigenetic mechanism for coordinate regulation of RNA Pol I- and II-transcribed genes that are critical for mammary epithelial proliferation, growth, and phenotype maintenance. Pharmacological inhibition of RUNX1 DNA binding causes transition to a mesenchymal phenotype, indicating that RUNX1 bookmarking of target genes contributes to stabilizing the normal breast epithelial phenotype.

Our findings are the first to identify coordinate control of cell growth-related ribosomal RNA (rRNA) genes and a large subset of cell proliferation/phenotype-related genes by RUNX1 in normal mammary epithelial cells. In addition to RUNX1 bookmarking of RNA Pol I-transcribed rRNA genes, RUNX1 is mitotically retained on RNA Pol II-transcribed genes that are important in breast epithelial cell growth and phenotype. One target gene of interest is hairy and enhancer of split-1 (*HES1*). Hes1 is a transcription factor which represses genes involved in cellular development, and is regulated primarily by NOTCH signaling, one of our top ten overlapping hallmark gene sets bookmarked by RUNX1 (Fig 5) [60,61]. HES1 was recently shown to have a prominent role in proliferation and invasion of breast cancer cells, and its silencing led to a downregulation of p-Akt signaling and ultimately prevented EMT[57]. Our findings indicate that RUNX1 stabilizes the normal mammary epithelial phenotype, in part, by bookmarking *HES1* and suppressing its expression.

Another important RNA Pol II-transcribed gene mitotically bookmarked by RUNX1 and critical for maintaining cellular phenotype is histone variant H2AFX (*H2AFX*). Silencing *H2AFX* in breast epithelial cells leads to induction of EMT through activation of

277 *SNAIL2/SLUG* and *TWIST1*[59]. We find a decrease in *H2AFX* expression and a
278 concomitant, significant increase in SNAIL2/SLUG expression upon inhibition of the
279 RUNX1-Cbfβ interaction. These data identify RUNX1 as a novel upstream regulator of
280 *H2AFX* expression; RUNX1 bookmarking and activation of H2AFX and subsequent
281 suppression of *SNAIL2/SLUG* prevents EMT in breast epithelial cells.

282 Several groups have shown that RUNX1 interacts with ERα at both enhancer
283 regions and transcriptional start sites (TSSs) for regulation of specific genes [22,54]. Our
284 ChIP-Seq results, coupled with publicly available data sets, reveal a novel finding: RUNX1
285 bookmarking of a subset of ERα-occupied, hormone-responsive genes, during mitosis
286 may be critical for maintenance of breast epithelial phenotype. Future studies will be
287 required to investigate mechanistic significance of this observation.

288 Our findings are the first to demonstrate that mitotic gene bookmarking contributes
289 to stabilizing the mammary epithelial phenotype. Equally important, our study shows that
290 inhibition of RUNX1 DNA binding specifically elicits an epithelial-to-mesenchymal
291 transition, indicating that mitotic gene bookmarking is a central epigenetic mechanism by
292 which RUNX1 maintains the epithelial phenotype. These findings are further supported
293 by RUNX1 mitotic occupancy of cell growth-related rRNA genes, and together highlight
294 key role(s) of RUNX1 in coordinating cell proliferation, growth and phenotype. Another
295 novel contribution of the current study is mitotic bookmarking of lncRNAs by a
296 transcription factor. RUNX1 was recently shown to regulate lncRNAs NEAT1 and NEAT2
297 (MALAT1)[55,62], lncRNAs with critical roles in the onset and progression of breast cancer[56].
298 Our findings show that, in addition to bookmarking protein coding genes, RUNX1
299 bookmarks several lncRNAs for post-mitotic regulation. It will be important to identify G1-

specific roles of RUNX1-bookmarked lncRNAs in maintaining the normal mammary epithelial phenotype and/or in the onset and progression of breast cancer.

In summary, this study establishes a novel epigenetic mechanism where RUNX1 mitotically bookmarks RNA Pol I- and II-transcribed genes for coordinate regulation of normal mammary epithelial proliferation, growth, and phenotype. Disruption of RUNX1 DNA binding leads to epithelial-to-mesenchymal transition, a key event in breast cancer onset, and validates the contribution of RUNX1 bookmarking to physiologically sustain the mammary epithelial phenotype.

MATERIALS AND METHODS

Cell Culture Techniques

Breast epithelial (MCF10A) cells were cultured in DMEM/F-12 50/50 mixture (Corning™, Corning, NY). Culturing media was also supplemented with horse serum to 5% (GIBCO, Grand Island, NY), human insulin to 10µg/mL (Sigma Aldrich, St. Louis, MO), human epidermal growth factor to 20ng/mL (PeproTech, Rocky Hill, NJ), cholera toxin to 100ng/mL (Thomas Scientific, Swedesboro, NJ), hydrocortisone to 500ng/mL (Sigma Aldrich, St. Louis, MO), Penicillin-Streptomycin to 100U/mL (Thermo Fisher Scientific, Ashville, NC), and L-Glutamine to 2mM (Thermo Fisher Scientific, Ashville, NC).

For mitotic arrest of parental MCF10A cells, culturing media was supplemented with 50ng/mL of Nocodazole (Sigma Aldrich, St. Louis, MO) and incubated with cells for 16hrs. Supplementing culturing media with equivalent volumes of DMSO (Sigma Aldrich, St. Louis, MO) served as a negative control. For DMSO-treated and mitotically arrested populations of MCF10A cells, harvests were conducted following the 16hr incubation. For G1 (released from mitotic arrest) populations of MCF10A cells, the nocodazole-supplemented culturing media was replaced with normal culturing media and incubated with cells for 3hrs. Following the 3hr incubation, released populations of cells were harvested for subsequent analysis.

Protein Expression and Localization

SDS-PAGE was performed to visualize protein expression within MCF10A cells. 8% SDS resolving gels and 4% stacking gels were prepared in-house (National Diagnostics, Atlanta, GA). Cell harvests were resuspended in RIPA buffer and incubated on ice for 30min. Following incubation, cell lysates were sonicated using Q700 Sonicator

(QSonica, Newtown, CT). Total sonication time for samples were 70 seconds, with 7 programed cycles of 10 seconds sonication at power setting 30 followed by 30 seconds of no sonication. Sonicated lysates were centrifuged at 15,000 rpm for 30min at 4℃. Protein concentration in the remaining supernatant was quantified using a Pierce™ BCA Protein Assay Kit (Thermo Fisher Scientific, Ashville, NC). Electrophoresis was performed at 160V for 15min followed by 200V for 45min. Overnight wet transfer of protein into PVDF membranes was performed at 30V for 18hr in 4℃. PVDF membranes were blocked at room temperature in 5% BSA in 1X TBST. Primary antibodies used for protein visualization were diluted 1:1000 and raised against UBF (sc-13125, Santa Cruz Biotechnology, Dallas, TX), RUNX1 (4334S, Cell Signaling Technologies, Danvers, MA), Cyclin B (4138S, Cell Signaling Technologies, Danvers, MA), Beta-Actin (3700S, Cell Signaling Technologies, Danvers, MA), and CDT1 (ab70829, AbCam, Cambridge, UK). Lamin B1 (ab16048, AbCam, Cambridge, UK) primary antibody was used at 1:2000 dilution for protein visualization. Primary antibodies were diluted in 5% BSA in 1XTBST and incubated with blots overnight at 4℃. Blots were washed four separate times with PBST or TBST. Goat anti-mouse IgG HRP conjugated (31460, Invitrogen, Carlsbad, CA) secondary antibody was incubated with blots at 1:5000 and incubated for 1hr at room temperature with mild agitation. Goat anti-rabbit IgG HRP conjugated (31430, Thermo Fisher Scientific, Ashville, NC) secondary antibody was incubated with blots at 1:1000, 1:2000, or 1:5000 and incubated for 1hr at room temperature with mild agitation. Blots were developed using Clarity Western ECL Substrate (Bio-Rad, Hercules, CA) following manufacturer's instructions. Blots were exposed to visualize protein and images were captured using Molecular Imager® Chemi doc™ XRS+ Imaging System (Bio-Rad,

Hercules, CA). Captured images were processed using Image Lab Software Version 5.1 (Bio-Rad, Hercules, CA).

Immunofluorescent microscopy was performed to observe distribution and localization of protein expression within MCF10A cells throughout all stages of mitosis and interphase. MCF10A cells were plated within a 6 well plate at 175,000 cells/mL on coverslips coated in gelatin (0.5% w/v solution in 1XPBS) and allowed to grow overnight. Coverslips were washed twice with sterile-filtered PBS at 4℃. Coverslips were then placed in room temperature fixative solution (1% MeOH-free Formaldehyde in PBS) for 10min. After a sterile-filtered PBS wash, coverslips were transferred to permeabilization solution (0.25% Triton X-100 in PBS) for 20min on ice. Following another sterile-filtered PBS wash, coverslips were then blocked in sterile-filtered PBS supplemented with bovine serum albumin (PBSA) at 0.5% w/v (Sigma Aldrich, St. Louis, MO). Coverslips were then incubated with primary antibody for 1hr at 37℃ in a humidified chamber. Primary antibodies were specific for RUNX1 at a dilution of 1:10 (4334S, Cell Signaling Technologies, Danvers, MA) and Upstream Binding Transcription Factor (UBF) at a dilution of 1:200 (F-9 sc-13125, Santa Cruz Biotechnology, Dallas, TX). Coverslips were washed four separate times in sterile-filtered PBSA following primary antibody incubation. Coverslips were then placed in secondary antibody for 1hr at 37℃ within a humidified chamber. Secondary antibodies used were goat anti-rabbit IgG conjugated with Alexa Fluor 488 (A-11070, Life Technologies, Carlsbad, CA) and goat anti-mouse IgG conjugated with Alexa Fluor 594 (A-11005, Life Technologies, Carlsbad, CA) diluted 1:800. Coverslips were then washed four times in sterile-filtered PBSA. Staining of the coverslips for DNA was performed with 1.0μg DAPI in 0.1% Triton X-100 and sterile-

379 filtered PBSA for 5min on ice. Stained coverslips were washed once in 0.1% Triton X-100
380 in sterile-filtered PBSA, then two times with sterile filtered PBS. Coverslips were mounted
381 onto slides using ProLong Gold Antifade Mountant (Thermo Fisher Scientific, Ashville,
382 NC). Images were captured using a Zeiss Axio Imager.Z2 fluorescent microscope and
383 Hamamatsu ORCA-R^2 C10600 digital camera. Images were processed using ZEN 2012
384 software.

385 Confocal microscopy was performed on slides prepared as described above.
386 MCF10A breast epithelial cells were initially imaged with a Zeiss LSM 510 META confocal
387 laser scanning microscope (Carl Zeiss Microscopy, LLC., Thornwood, NY, USA) for a
388 preliminary study to assess potential colocalization. At a later time, additional samples
389 were imaged with a Nikon A1R-ER laser scanning confocal microscope (Nikon, Melville,
390 NY,USA) for complete colocalization analysis. Images were acquired with the resonant
391 scanner at a frame size of 1024 X 1024 pixels with 8X averaging. Fluorescently labeled
392 samples were excited by laser lines sequentially imaged in channel series mode. The
393 DAPI signal was excited with a 405 nm laser and collected with a 425-475 nm band pass
394 filter, Alexa 488 was excited with a 488 nm laser and collected with a 500-550 nm band
395 pass filter, and Alexa 568 with a 561 nm laser and collected with a 570-620 nm band pass
396 filter. Images were captured with a Plan-Fluor 40X (1.3 NA) objective lens. The confocal
397 pinhole was initially set to 1.2 Airy Unit diameter for the 561 nm excitation giving an optical
398 section thickness of 0.41 µm. Images were acquired at 12-bit data depth, and all settings,
399 including laser power, amplifier gain, and amplifier offset were established using a look-
400 up table to provide an optimal gray-scale intensities. All images were acquired using
401 matching imaging parameters.

Images were acquired with at 40X objective were subject to colocalization analysis via Volocity version 6.3.0 (Perkin Elmer, Waltham, MA, USA). Images were opened in the colocalization tab. Cell nuclei, indicated by the DAPI signal, were circled via the ROI tool. At least 15 interphase and 15 metaphase cells were identified within captured images and appropriate thresholds were manually determined to eliminate background fluorescence for calculating Pearsons and Manders correlation coefficients between RUNX1 and UBF.

Images were also viewed in NIS Elements version 5.02.01 and analyzed using the line profiling tool. Overlaying DAPI, RUNX1, and UBF fluorescent intensities from individual channels along the line profile revealed overlapping peak intensities between the RUNX1 and UBF channels, thus indicating colocalization.

Core binding factor – Beta (CBFβ) inhibitors AI-4-88 and AI-14-91 were given to us from John H. Bushweller (University of Virginia) and used to evaluate RUNX1 DNA-binding inhibition in MCF10A cells. Protein synthesis evaluation by immunofluorescence was conducted following manufacturer protocol (K715-100, BioVision, San Francisco, CA).

Molecular Techniques

Total RNA was isolated from MCF10A cells using TRIzol™ Reagent (Invitrogen, Carlsbad, CA) and Direct-Zol™ RNA MiniPrep isolation kit (Zymo Research, Irvine, CA) following manufacturer instructions. cDNA was created using SuperScript IV® First-Strand Synthesis System for RT-PCR (ThermoFisher, Asheville, NC). Resulting samples were quantified on a Qubit 2.0 Fluorometer (Invitrogen, Carlsbad, CA) and diluted to 500pg/μL. Equal amounts of DNA template were loaded for samples analyzed by qPCR.

Chromatin Immunoprecipitation was conducted on asynchronous (Asynch), mitotically arrested (M), and released from mitosis (G1) MCF10A breast epithelial cells. Cells were fixed with 1% v/v MeOH-free Formaldehyde in 1XPBS for 10min at room temperature. Formaldehyde fixation was neutralized using 2.5M Glycine and incubated with cells for 5min at room temperature. Two washes with 1XPBS supplemented with cOmplete™ EDTA-free Protease Inhibitor Cocktail (Sigma Aldrich, Saint Louis, MO) and MG-132 (Calbiochem-Millipore Sigma, Burlington, MA) were performed. For asynchronous and G1 populations of cells, culture dishes were scraped to collect fixated lysate. Mitotic cells were isolated using a mitotic shake off. Mitotic cells were spun down at 1500rpm x 5min, resuspended in 1% v/v MeOH-free Formaldehyde in 1XPBS, and neutralized with 2.5M Glycine for 5min. Fixed harvests were centrifuged at 1500rpm x 5min (4°C) and the supernatant was discarded. All fixed cell pellets were flash frozen in liquid nitrogen and stored at -80°C until lysis.

Fixed cell pellets were thawed on ice. Once thawed, pellets were lysed in a nuclear lysis buffer supplemented with cOmplete™ EDTA-free Protease Inhibitor Cocktail (Sigma Aldrich, Saint Louis, MO) and MG-132 (Calbiochem-Millipore Sigma, Burlington, MA) with a volume that was approximately 5X the volume of pellet. Pellets were incubated in nuclear lysis buffer for 30min before being flash frozen down in liquid nitrogen. Lysates were thawed at room temperature but not allowed to reach room temperature. Sonication of the lysates were performed using a S220 focused ultra-sonicator (Covaris, Matthews, NC). Sonication parameters for each population of cells was as follows: Peak Watt 140W, Duty Factor 10, Cycle/Burst 200. M and G1 populations of cells were sonicated for 28min total whereas asynchronous populations of cells were sonicated for 36min. All samples

were sonicated at 6°C. Following sonication, aliquots were spun down at 15,000rpm x 10min and 4°C. Following the spin, the resulting supernatants were pooled together and analyzed.

Sonicated lysate was boiled in 100°C for 15min with NaCl and elution buffer. Boiled lysate was allowed to cool and treated with RNaseA (10ug/uL) for 10min at 37°C. DNA was isolated using PureLink™ PCR Purification Kit (K310001, ThermoFisher, Ashville, NC) following manufacturer recommendations. Resulting DNA was quantified via nanodrop and 1.0-2.0ug was run on a 1.5% agarose gel to observe sonication results prior to generating ChIP reactions. Resulting DNA was also quantified via Qubit 2.0 Fluorometer (Invitrogen, Carlsbad, CA) and analyzed by using a High Sensitivity DNA Kit on a Bioanalyzer 2100 (Agilent, Santa Clara, CA).

For chromatin immunoprecipitation (ChIP) reactions, 150ug of sonicated chromatin was incubated with 10ug of RUNX1 antibody (4336BF, Cell Signaling Technologies, Danvers, MA), diluted 1:10 in IP dilution buffer, and incubated overnight (16-18hrs) at 4°C with mild agitation. Following incubation, 150uL of Protein A/G magnetic beads (Thermo Scientific – Pierce, Waltham, MA) per ug of antibody used were added to each IP reaction and incubated for 2-4hrs at 4°C with mild agitation. Beads were isolated from solution using a powerful magnet, and washed two times in two separate IP wash buffers. Lastly, beads were resuspended in an elution buffer and agitated in a thermomixer (Eppendorf, Hamburg, Germany) or vortexer at 1000rpm x 30min at room temperature. This elution step was repeated on the beads. Using a magnet, beads were discarded and the resulting supernatant was incubated with NaCl overnight (16-18hrs) at 67°C to reverse formaldehyde crosslinks. DNA from RUNX1 ChIP samples were purified

using PureLink™ PCR Purification Kit (K310001, ThermoFisher, Ashville, NC) following manufacturer recommendations.

ChIP libraries were generated using Accel-NGS® 2S Plus DNA Library kit (Swift Biosciences, Ann Arbor, MI) following manufacturers protocol. Input and RUNX1 ChIP samples were normalized to 1ng prior to library generation. Libraries were amplified in an optional PCR step for 12 total cycles. Finalized libraries were double size selected using AMPure XP beads (0.8X and 0.2X volume ratios to sample), resulting in the majority fragments sized between 250-400bp. Next generation sequencing of pooled ChIP libraries was performed by the University of Vermont Cancer Center - Vermont Integrated Genomics Resource (VIGR).

Bioinformatics Analyses

Because we were specifically investigating rDNA, a customized build of hg38 was constructed that included normally masked regions of rDNA (Gencode U13369). Since some (although not complete) rDNA sequence is present in the hg38 assembly, we masked all parts of hg38 that would normally be attributed to rDNA sequences (bedtools v2.25.0 maskfasta). Finally, we appended the complete rDNA sequence as a “unique” chromosome (chrU13369.1) to the masked hg38 FASTA resulting in the hg38_rDNA assembly used for analysis.

Single-end, 50bp reads (SE50) were processed pre-alignment by removing adapter reads (Cutadapt v1.6) and trimming low quality base calls from both ends (FASTQ Quality Trimmer 1.0.0; min score >= 20, window of 10, and step size of 1). Resulting reads were aligned to hg38_rDNA (STAR v2.4; splicing disabled with '--alignIntronMax 1'). Next, we

called peaks and generated fold-enrichment (FE) bedGraph files (MACS2 v2.1.0.20140616; callpeak at p-value e-5; and bdgcmp with FE method) [63]. Irreproducible Discovery Rate (IDR) was conducted using unpooled replicates with all peaks in pooled samples passing an IDR cutoff of 0.5 [64]. To reduce artificial peaks, we calculated strand cross-correlation for all peaks at a shift of 95 bp (the mean observed fragment size of 180 bp minus the read size of 85bp) and unshifted [65]. We eliminated peaks that exhibited low shifted correlation (shifted correlation <.7) and those that exhibited high unshifted correlation relative to shifted (shifted – unshifted correlation < .1). This increased retrieval of the RUNX1 motif and improved agreement with other RUNX1 datasets. Passing peaks were annotated separately to mRNA and lncRNA transcript start sites (TSSs) using GENCODE v27 with a distance cutoff of 5000 bp. Regional distribution of peaks was determined using the same annotation reference limited to the "basic" tag for exons and promoters.

ACKNOWLEDGEMENTS

The authors would like to thank John H. Bushweller, PhD (University of Virginia), who created and gifted us Core binding factor – Beta (CBFβ) inhibitors AI-4-88 and AI-14-91 to conduct RUNX1 inhibition experiments for this study. Confocal imaging and colocalization analysis were performed by Nicole Bouffard in the Microscopy Imaging Center at the University of Vermont College of Medicine. The authors would also like to thank Scott Tighe, Pheobe Kehoe, and Jessica Hoffman for performing next generation sequencing of samples (Vermont Integrated Genomics Resource (VIGR) at the University of Vermont Cancer Center). The authors also thank Roxana del Rio-Guerra, Ph.D of the

UVM Flow Cytometry and Cell Sorting Facility for analysis of samples by FACS. The authors would also like to thank Alan Howe, Ph.D. (University of Vermont) for his Phalloidin reagent used in immunofluorescence microscopy experiments.

COMPETING INTERESTS

No competing interests declared.

FUNDING

This work was supported by NIH grants NCI P01 CA082834 (to G.S. Stein and J.L. Stein), R01 CA139322 (to G.S. Stein), R37 DE012528 (to J.B. Lian), NCI F32 CA220935 (to A.J. Fritz, G.S. Stein, and J.L. Stein), U01 CA196383 (to J.L. Stein), and the Charlotte Perelman Fund for Cancer Research (to G.S. Stein). The confocal microscopy work described in this manuscript was supported by Award Number 1S10RR019246 from the National Center for Research Resources for purchase of the Zeiss 510 META confocal scanning laser microscope and NIH award number 1S10OD025030-01 for purchase of the Nikon A1R-ER point scanning confocal microscope from the National Center for Research Resources. FACS experiments performed at the Harry Hood Bassett Flow Cytometry and Cell Sorting Facility, University of Vermont College of Medicine were supported by NIH S10-ODO18175.

DATA AVAILABILITY

GEO accession number for the sequencing data generated in this study is GSE121370.

REFERENCES

1 Hanahan, D. & Weinberg, R. A. Hallmarks of cancer: the next generation. *Cell* **144**, 646-674, doi:10.1016/j.cell.2011.02.013 (2011).

2 Micalizzi, D. S., Farabaugh, S. M. & Ford, H. L. Epithelial-mesenchymal transition in cancer: parallels between normal development and tumor progression. *Journal of mammary gland biology and neoplasia* **15**, 117-134, doi:10.1007/s10911-010-9178-9 (2010).

3 Schmalhofer, O., Brabletz, S. & Brabletz, T. E-cadherin, beta-catenin, and ZEB1 in malignant progression of cancer. *Cancer metastasis reviews* **28**, 151-166, doi:10.1007/s10555-008-9179-y (2009).

4 Taube, J. H. *et al.* Core epithelial-to-mesenchymal transition interactome gene-expression signature is associated with claudin-low and metaplastic breast cancer subtypes. *Proc Natl Acad Sci U S A* **107**, 15449-15454, doi:10.1073/pnas.1004900107 (2010).

5 Yang, J. & Weinberg, R. A. Epithelial-mesenchymal transition: at the crossroads of development and tumor metastasis. *Developmental cell* **14**, 818-829, doi:10.1016/j.devcel.2008.05.009 (2008).

6 Dowdy, C. R. *et al.* Definitive hematopoiesis requires Runx1 C-terminal-mediated subnuclear targeting and transactivation. *Hum Mol Genet* **19**, 1048-1057, doi:10.1093/hmg/ddp568 (2010).

7 Hilton, M. J. *et al.* Notch signaling maintains bone marrow mesenchymal progenitors by suppressing osteoblast differentiation. *Nature medicine* **14**, 306-314, doi:10.1038/nm1716 (2008).

8 Huang, H. *et al.* A Src family kinase-Shp2 axis controls RUNX1 activity in megakaryocyte and T-lymphocyte differentiation. *Genes & development* **26**, 1587-1601, doi:10.1101/gad.192054.112 (2012).

9 Ito, K. *et al.* RUNX3 attenuates beta-catenin/T cell factors in intestinal tumorigenesis. *Cancer cell* **14**, 226-237, doi:10.1016/j.ccr.2008.08.004 (2008).

10 Ito, Y. RUNX genes in development and cancer: regulation of viral gene expression and the discovery of RUNX family genes. *Advances in cancer research* **99**, 33-76, doi:10.1016/s0065-230x(07)99002-8 (2008).

11 Ito, Y., Bae, S. C. & Chuang, L. S. The RUNX family: developmental regulators in cancer. *Nat Rev Cancer* **15**, 81-95, doi:10.1038/nrc3877 (2015).

12 Ito, Y. & Miyazono, K. RUNX transcription factors as key targets of TGF-beta superfamily signaling. *Current opinion in genetics & development* **13**, 43-47 (2003).

13 Lam, K. & Zhang, D. E. RUNX1 and RUNX1-ETO: roles in hematopoiesis and leukemogenesis. *Frontiers in bioscience (Landmark edition)* **17**, 1120-1139 (2012).

14 Min, B. *et al.* Identification of RUNX3 as a component of the MST/Hpo signaling pathway. *Journal of cellular physiology* **227**, 839-849, doi:10.1002/jcp.22887 (2012).

15 Pratap, J. *et al.* Runx2 transcriptional activation of Indian Hedgehog and a downstream bone metastatic pathway in breast cancer cells. *Cancer Res* **68**, 7795-7802, doi:10.1158/0008-5472.CAN-08-1078 (2008).

16 Tai, P. W. L. *et al.* Genome-wide DNase hypersensitivity, and occupancy of RUNX2 and CTCF reveal a highly dynamic gene regulome during MC3T3 pre-osteoblast differentiation. *PloS one* **12**, e0188056, doi:10.1371/journal.pone.0188056 (2017).

17 VanOudenhove, J. J. *et al.* Transient RUNX1 Expression during Early Mesendodermal Differentiation of hESCs Promotes Epithelial to Mesenchymal Transition through TGFB2 Signaling. *Stem Cell Reports* **7**, 884-896, doi:10.1016/j.stemcr.2016.09.006 (2016).

18 Vega, O. A. *et al.* Wnt/beta-Catenin Signaling Activates Expression of the Bone-Related Transcription Factor RUNX2 in Select Human Osteosarcoma Cell Types. *Journal of cellular biochemistry* **118**, 3662-3674, doi:10.1002/jcb.26011 (2017).

19 Zheng, L. *et al.* Runx2/DICER/miRNA Pathway in Regulating Osteogenesis. *Journal of cellular physiology* **232**, 182-191, doi:10.1002/jcp.25406 (2017).

20 Browne, G. *et al.* MicroRNA-378-mediated suppression of Runx1 alleviates the aggressive phenotype of triple-negative MDA-MB-231 human breast cancer cells. *Tumour Biol* **37**, 8825-8839, doi:10.1007/s13277-015-4710-6 (2016).

21 Browne, G. *et al.* Runx1 is associated with breast cancer progression in MMTV-PyMT transgenic mice and its depletion in vitro inhibits migration and invasion. *J Cell Physiol* **230**, 2522-2532, doi:10.1002/jcp.24989 (2015).

22 Chimge, N. O. *et al.* RUNX1 prevents oestrogen-mediated AXIN1 suppression and beta-catenin activation in ER-positive breast cancer. *Nature communications* **7**, 10751, doi:10.1038/ncomms10751 (2016).

23 Hong, D. *et al.* Runx1 stabilizes the mammary epithelial cell phenotype and prevents epithelial to mesenchymal transition. *Oncotarget* **8**, 17610-17627, doi:10.18632/oncotarget.15381 (2017).

24 Recouvreux, M. S. *et al.* RUNX1 and FOXP3 interplay regulates expression of breast cancer related genes. *Oncotarget* **7**, 6552-6565, doi:10.18632/oncotarget.6771 (2016).

25 Comprehensive molecular portraits of human breast tumours. *Nature* **490**, 61-70, doi:10.1038/nature11412 (2012).

26 Banerji, S. *et al.* Sequence analysis of mutations and translocations across breast cancer subtypes. *Nature* **486**, 405-409, doi:10.1038/nature11154 (2012).

27 Ellis, M. J. *et al.* Whole-genome analysis informs breast cancer response to aromatase inhibition. *Nature* **486**, 353-360, doi:10.1038/nature11143 (2012).

28 Liu, Y. N. *et al.* Regulatory mechanisms controlling human E-cadherin gene expression. *Oncogene* **24**, 8277-8290, doi:10.1038/sj.onc.1208991 (2005).

29 John, S. & Workman, J. L. Bookmarking genes for activation in condensed mitotic chromosomes. *Bioessays* **20**, 275-279, doi:10.1002/(SICI)1521-1878(199804)20:4<275::AID-BIES1>3.0.CO;2-P (1998).

30 Raccaud, M. & Suter, D. M. Transcription factor retention on mitotic chromosomes: regulatory mechanisms and impact on cell fate decisions. *FEBS letters* **592**, 878-887, doi:10.1002/1873-3468.12828 (2018).

31 Sarge, K. D. & Park-Sarge, O. K. Gene bookmarking: keeping the pages open. *Trends Biochem Sci* **30**, 605-610, doi:10.1016/j.tibs.2005.09.004 (2005).

32 Caravaca, J. M. *et al.* Bookmarking by specific and nonspecific binding of FoxA1 pioneer factor to mitotic chromosomes. *Genes Dev* **27**, 251-260, doi:10.1101/gad.206458.112 (2013).

33 Deluz, C. *et al.* A role for mitotic bookmarking of SOX2 in pluripotency and differentiation. *Genes & development* **30**, 2538-2550, doi:10.1101/gad.289256.116 (2016).

34 Kadauke, S. *et al.* Tissue-specific mitotic bookmarking by hematopoietic transcription factor GATA1. *Cell* **150**, 725-737, doi:10.1016/j.cell.2012.06.038 (2012).

35 Lake, R. J., Tsai, P. F., Choi, I., Won, K. J. & Fan, H. Y. RBPJ, the major transcriptional effector of Notch signaling, remains associated with chromatin throughout mitosis, suggesting a role in mitotic bookmarking. *PLoS Genet* **10**, e1004204, doi:10.1371/journal.pgen.1004204 (2014).

36 Liu, Y. *et al.* Widespread Mitotic Bookmarking by Histone Marks and Transcription Factors in Pluripotent Stem Cells. *Cell Rep* **19**, 1283-1293, doi:10.1016/j.celrep.2017.04.067 (2017).

37 Ali, S. A. *et al.* Phenotypic transcription factors epigenetically mediate cell growth control. *Proc Natl Acad Sci U S A* **105**, 6632-6637, doi:10.1073/pnas.0800970105 (2008).

38 Young, D. W. *et al.* Mitotic occupancy and lineage-specific transcriptional control of rRNA genes by Runx2. *Nature* **445**, 442-446, doi:10.1038/nature05473 (2007).

39 Young, D. W. *et al.* Mitotic retention of gene expression patterns by the cell fate-determining transcription factor Runx2. *Proc Natl Acad Sci U S A* **104**, 3189-3194, doi:10.1073/pnas.0611419104 (2007).

40 Zaidi, S. K. *et al.* Mitotic partitioning and selective reorganization of tissue-specific transcription factors in progeny cells. *Proceedings of the National Academy of Sciences of the United States of America* **100**, 14852-14857, doi:10.1073/pnas.2533076100 (2003).

41 Shrivastava, T. *et al.* Structural basis of Ets1 activation by Runx1. *Leukemia* **28**, 2040-2048, doi:10.1038/leu.2014.111 (2014).

42 Carlton, A. L. *et al.* Small molecule inhibition of the CBFbeta/RUNX interaction decreases ovarian cancer growth and migration through alterations in genes related to epithelial-to-mesenchymal transition. *Gynecol Oncol* **149**, 350-360, doi:10.1016/j.ygyno.2018.03.005 (2018).

43 Illendula, A. *et al.* Small Molecule Inhibitor of CBFbeta-RUNX Binding for RUNX Transcription Factor Driven Cancers. *EBioMedicine* **8**, 117-131, doi:10.1016/j.ebiom.2016.04.032 (2016).

44 Kim, W. *et al.* RUNX1 is essential for mesenchymal stem cell proliferation and myofibroblast differentiation. *Proc Natl Acad Sci U S A* **111**, 16389-16394, doi:10.1073/pnas.1407097111 (2014).

45 Ozaki, T., Nakagawara, A. & Nagase, H. RUNX Family Participates in the Regulation of p53-Dependent DNA Damage Response. *International journal of genomics* **2013**, 271347, doi:10.1155/2013/271347 (2013).

46 Satoh, Y. *et al.* C-terminal mutation of RUNX1 attenuates the DNA-damage repair response in hematopoietic stem cells. *Leukemia* **26**, 303-311, doi:10.1038/leu.2011.202 (2012).

47 Wang, C. Q. *et al.* Disruption of Runx1 and Runx3 leads to bone marrow failure and leukemia predisposition due to transcriptional and DNA repair defects. *Cell Rep* **8**, 767-782, doi:10.1016/j.celrep.2014.06.046 (2014).

48 Wu, D., Ozaki, T., Yoshihara, Y., Kubo, N. & Nakagawara, A. Runt-related transcription factor 1 (RUNX1) stimulates tumor suppressor p53 protein in response to DNA damage through complex formation and acetylation. *The Journal of biological chemistry* **288**, 1353-1364, doi:10.1074/jbc.M112.402594 (2013).

49 Cargnello, M., Tcherkezian, J. & Roux, P. P. The expanding role of mTOR in cancer cell growth and proliferation. *Mutagenesis* **30**, 169-176, doi:10.1093/mutage/geu045 (2015).

50 Ciruelos Gil, E. M. Targeting the PI3K/AKT/mTOR pathway in estrogen receptor-positive breast cancer. *Cancer treatment reviews* **40**, 862-871, doi:10.1016/j.ctrv.2014.03.004 (2014).

51 Feng, Y., Manka, D., Wagner, K. U. & Khan, S. A. Estrogen receptor-alpha expression in the mammary epithelium is required for ductal and alveolar morphogenesis in mice. *Proc Natl Acad Sci U S A* **104**, 14718-14723, doi:10.1073/pnas.0706933104 (2007).

52 Mallepell, S., Krust, A., Chambon, P. & Brisken, C. Paracrine signaling through the epithelial estrogen receptor alpha is required for proliferation and morphogenesis in the mammary gland. *Proc Natl Acad Sci U S A* **103**, 2196-2201, doi:10.1073/pnas.0510974103 (2006).

53 Mueller, S. O., Clark, J. A., Myers, P. H. & Korach, K. S. Mammary gland development in adult mice requires epithelial and stromal estrogen receptor alpha. *Endocrinology* **143**, 2357-2365, doi:10.1210/endo.143.6.8836 (2002).

54 Stender, J. D. *et al.* Genome-wide analysis of estrogen receptor alpha DNA binding and tethering mechanisms identifies Runx1 as a novel tethering factor in receptor-mediated transcriptional activation. *Mol Cell Biol* **30**, 3943-3955, doi:10.1128/MCB.00118-10 (2010).

55 Gutschner, T., Hammerle, M. & Diederichs, S. MALAT1 -- a paradigm for long noncoding RNA function in cancer. *Journal of molecular medicine (Berlin, Germany)* **91**, 791-801, doi:10.1007/s00109-013-1028-y (2013).

56 Yu, X., Li, Z., Zheng, H., Chan, M. T. & Wu, W. K. NEAT1: A novel cancer-related long non-coding RNA. *Cell Prolif* **50**, doi:10.1111/cpr.12329 (2017).

57 Li, X., Cao, Y., Li, M. & Jin, F. Upregulation of HES1 Promotes Cell Proliferation and Invasion in Breast Cancer as a Prognosis Marker and Therapy Target via the AKT Pathway and EMT Process. *Journal of Cancer* **9**, 757-766, doi:10.7150/jca.22319 (2018).

58 Strom, A., Arai, N., Leers, J. & Gustafsson, J. A. The Hairy and Enhancer of Split homologue-1 (HES-1) mediates the proliferative effect of 17beta-estradiol on breast cancer cell lines. *Oncogene* **19**, 5951-5953 (2000).

59 Weyemi, U. *et al.* Twist1 and Slug mediate H2AX-regulated epithelial-mesenchymal transition in breast cells. *Cell cycle (Georgetown, Tex.)* **15**, 2398-2404, doi:10.1080/15384101.2016.1198864 (2016).

60 Kageyama, R., Ohtsuka, T. & Kobayashi, T. The Hes gene family: repressors and oscillators that orchestrate embryogenesis. *Development (Cambridge, England)* **134**, 1243-1251, doi:10.1242/dev.000786 (2007).

61 Rani, A., Greenlaw, R., Smith, R. A. & Galustian, C. HES1 in immunity and cancer. *Cytokine & growth factor reviews* **30**, 113-117, doi:10.1016/j.cytogfr.2016.03.010 (2016).

62 Barutcu, A. R. *et al.* RUNX1 contributes to higher-order chromatin organization and gene regulation in breast cancer cells. *Biochim Biophys Acta* **1859**, 1389-1397, doi:10.1016/j.bbagrm.2016.08.003 (2016).

63 Zhang, Y. *et al.* Model-based analysis of ChIP-Seq (MACS). *Genome Biol* **9**, R137, doi:10.1186/gb-2008-9-9-r137 (2008).

64 Li, Q., Brown, J. B., Huang, H. & Bickel, P. J. Measuring reproducibility of high-throughput experiments.

65 Landt, S. G. *et al.* ChIP-seq guidelines and practices of the ENCODE and modENCODE consortia. *Genome research* **22**, 1813-1831, doi:10.1101/gr.136184.111 (2012).

FIGURE LEGENDS

Figure 1. RUNX1 associates with DNA during interphase and remains bound throughout mitosis in the form of major and minor foci. Representative immunofluorescent images of interphase and mitotic MCF10A breast epithelial cells. Mitotic cells were further classified into substages of mitosis based on DAPI topology. RUNX1 – Green (top row), DAPI – Blue (second row from top). Merged channel images (third row from top) contain an outlined region magnified in the bottom row labeled "inset". White arrows highlight major Runx1 foci on chromatin.

Figure 2. RUNX1 occupies protein coding genes and long non-coding RNAs across asynchronous, mitotic, and G1 populations of MCF10A breast epithelial cells. A) Experimental schematic depicting mitotic arrest and harvest of each treated MCF10A cell populations: Asynchronous – A, Mitotic – M, and Released – G1. B) Western blot of each harvested MCF10A population for cell cycle specific markers to evaluate mitotic arrest and synchronization procedure. C) Fluorescently activated cell sorting (FACS) analysis of harvested A, M, and G1 MCF10A cells to determine mitotic purity and DNA content (n=3 biological replicates per group). D) Heatmaps showing peaks called between A, M, and G1 MCF10A cells (left, middle, and right respectively). E) Venn diagrams illustrating the number of protein coding genes (left diagram) and lncRNAs (right diagram) identified within and between A, M, and G1 MCF10A populations. F) Motif analysis of A, M, and G1 MCF10A cells

740 **Figure 3. RUNX1 colocalizes with RNA Pol I subunit, upstream binding factor**
741 **(UBF) on mitotic chromatin.** A) Immunofluorescence microscopy images of RUNX1
742 (green – top row), UBF (red – 2nd row from top), DAPI (blue – 2nd row from bottom), and
743 the three channels merged (bottom row) in MCF10A cells. Images were captured of
744 spontaneously dividing MCF10A cells in different substages of mitosis. B)
745 Representative images of line profiles taken on interphase vs metaphase cells (n=15
746 each).

747

748 **Figure 4. RUNX1 bookmarks rDNA promoter repeat regions and affects both pre-**
749 **rRNA and global protein expression.** A) ChIP-Seq tracks of A, M, and G1 (top,
750 middle, bottom respectively) MCF10A cells mapped against rDNA repeat regions. B)
751 Representative immunofluorescence images of the active compound (AI-14-91)-treated
752 MCF10A cells in prophase and metaphase are shown. A substantial decrease in
753 smaller RUNX1 foci (green) during mitosis is observed when compared to the inactive
754 (AI-4-88) compound. Large RUNX1 foci that colocalize with UBF (red) are detectable at
755 all substages of mitosis (white arrows) in the presence of either active or inactive
756 compounds. C) qRT-PCR data of pre-rRNA in actively proliferating MCF10A cells
757 treated with either active (AI-14-91) or inactive (AI-4-88) compounds for 6, 12, 24, or
758 48hrs. Expression of pre-rRNA was normalized relative to Beta Actin expression. D)
759 Representative fluorescence microscopy images of global protein synthesis occurring
760 within MCF10A cells treated with either AI-4-88 (left) or AI-14-91 (right) for 24hr at
761 20μM. Intensity of red fluorescence at 580nm emission indicates nascent protein
762 synthesis. All images were taken with 1000ms exposures.

Figure 5. RUNX1 bookmarks RNA Pol II-transcribed genes involved in maintenance of breast epithelial phenotype. A) Gene Set Enrichment (GSE) analysis from interrogating mitotically bookmarked genes (i.e. RUNX1 mitotically occupied) against Hallmark Gene sets from Molecular Signatures Database (MSigDB). The top 10 most significantly overlapping gene sets are shown from top to bottom. B) Scatter plot of genes identified to be up or down regulated in response to estradiol treatment, that are also bound by estrogen receptor α (ERα) and RUNX1 (empty circles, blue for downregulated and red for upregulated). Scatter plot also illustrates up or down regulated genes in response to estradiol treatment that are bound by ERα and mitotically bookmarked by RUNX1 (filled in circles, blue for downregulated and red for upregulated). C) Top panel: ChIP-Seq tracks of *HES1* (left) and *H2AFX* (right) from asynchronous (top-red), mitotic (middle-green), and G1 (bottom-blue). Bottom panel: qRT-PCR data of *HES1* (left) and *H2AFX* (right) in asynchronous MCF10A cells treated with either active (AI-14-91) or inactive (AI-4-88) inhibitors for 6hr, 12hr, 24hr and 48hr at 20μM. Expression of target genes were normalized relative to beta actin.

Figure 6. Disrupting RUNX1 mitotic gene bookmarking in MCF10A cells leads to a transformed cellular phenotype and EMT. A) Phase contrast microscopy images of MCF10A cells treated with AI-4-88 or AI-14-91 for 48hr at 20μM. Left panel – 4X magnification, middle panel – 20X magnification, right panel – 40X magnification. Outlined square in middle panel is the resulting 40X magnification in the right panel. B) Top Panel: Experimental schematic depicting treatment schedule for the “crisis” and

786 “recovery” stages. Bottom Panel: Phase contrast microscopy images from Day 0, 1, and
787 2 of crisis where MCF10A cells were treated with AI-14-91 at 20μM (top – left, middle,
788 right respectively). Phase contrast images from Day 0, 4, and 7 of recovery following a
789 media replacement. C) Morphological changes upon inhibition of RUNX1-CBFβ
790 interaction are confirmed by examining localization of the cytoskeletal protein F-actin.
791 When compared to inactive compound (top panel), cells treated with active compound
792 show substantial alterations in cytoarchitecture (bottom panel). D) Western blot for
793 epithelial marker E-Cadherin (top row), mesenchymal marker Vimentin (middle row),
794 and loading control beta actin (bottom row) in MCF10A whole cell lysates harvested
795 from cells treated with either inactive AI-4-88 (88) or active AI-14-91 (91) inhibitors at
796 20μM for either 6, 12, 24, or 48hrs. E) qRT-PCR of target genes *p21* (RUNX1 regulated)
797 and *SNAI2* (EMT inducing transcription factor) within asynchronous MCF10A cells
798 treated with either inactive AI-4-88 (88) or active AI-14-91 (91) inhibitors at 20μM for
799 either 6, 12, 24, or 48hrs. Expression of target genes were normalized relative to beta
800 actin.

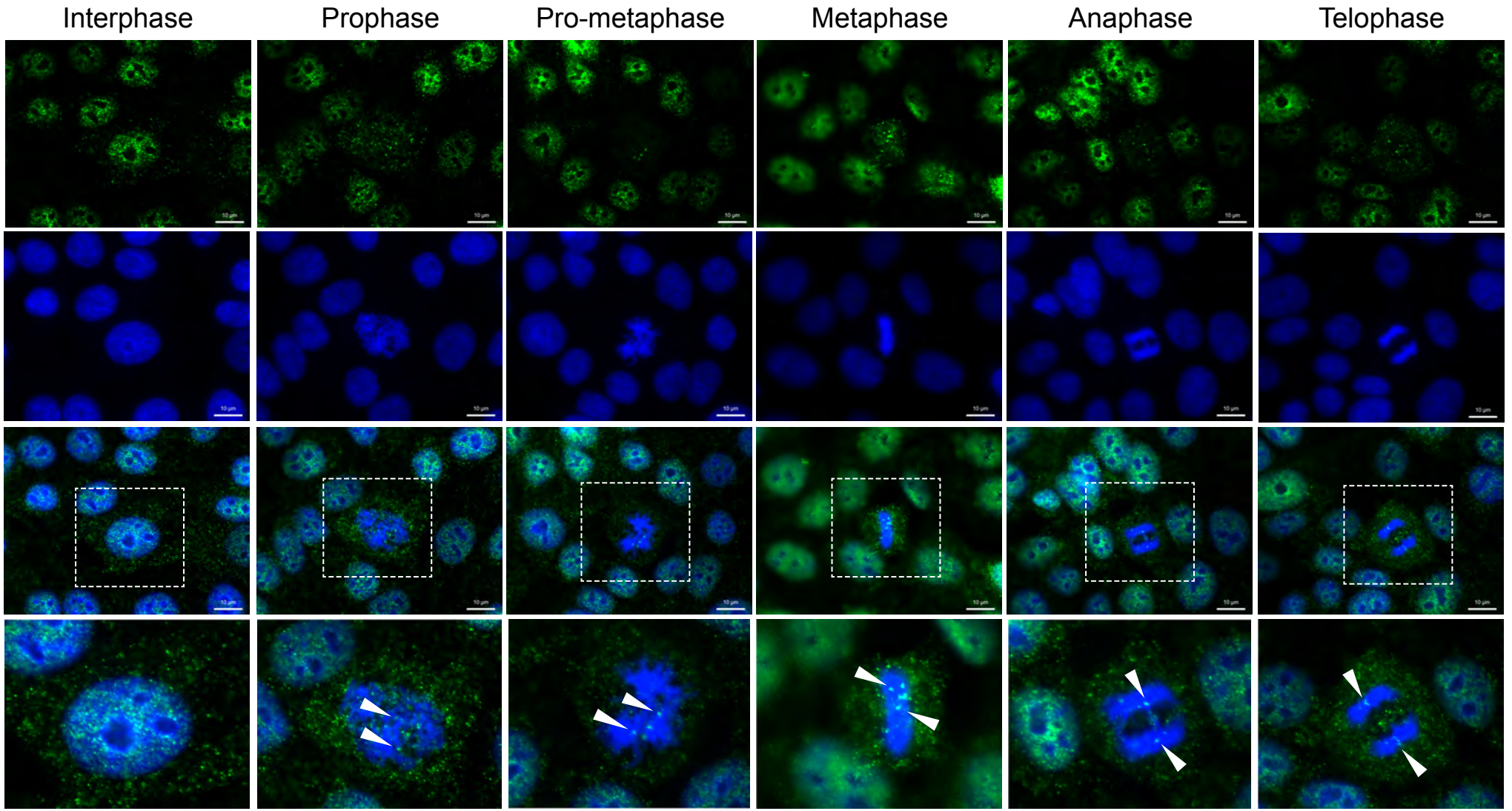
Interphase
Prophase
Pro-metaphase
Metaphase
Anaphase
Telophase
RUNX1
DAPI
MERGED
INSET

Figure 1

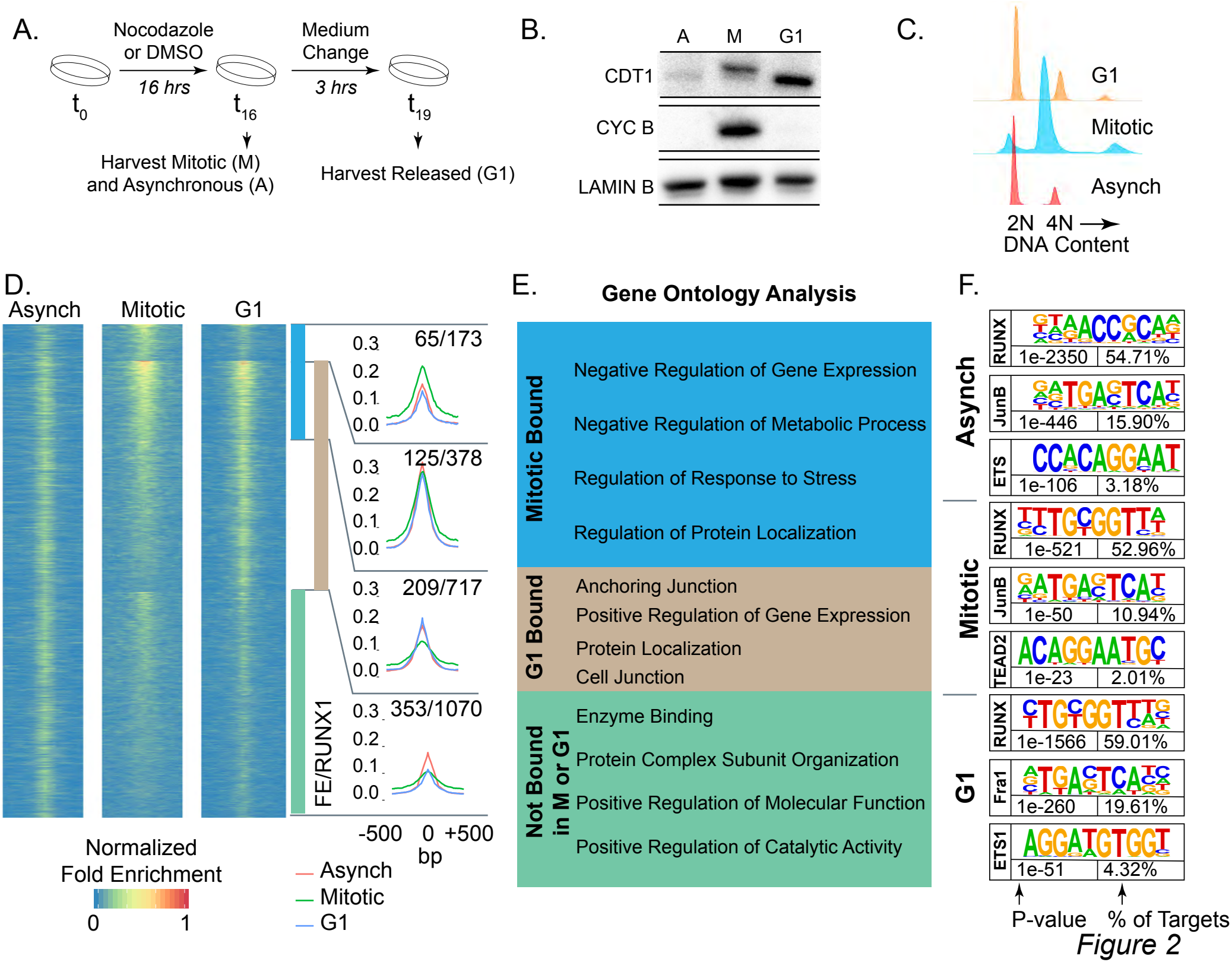
A.
Nocodazole or DMSO
16 hrs
Medium Change
3 hrs
t0
t16
t19
Harvest Mitotic (M) and Asynchronous (A)
Harvest Released (G1)
B.
A
M
G1
CDT1
CYC B
LAMIN B
C.
G1
Mitotic
Asynch
2N 4N
DNA Content
D.
Asynch
Mitotic
G1
65/173
125/378
209/717
353/1070
FE/RUNX1
0.3
0.2
0.1
0.0
-500 0 +500
bp
Normalized Fold Enrichment
0 1
Asynch
Mitotic
G1
E.
Gene Ontology Analysis
Mitotic Bound
Negative Regulation of Gene Expression
Negative Regulation of Metabolic Process
Regulation of Response to Stress
Regulation of Protein Localization
G1 Bound
Anchoring Junction
Positive Regulation of Gene Expression
Protein Localization
Cell Junction
Not Bound in M or G1
Enzyme Binding
Protein Complex Subunit Organization
Positive Regulation of Molecular Function
Positive Regulation of Catalytic Activity
F.
Asynch
RUNX
1e-2350
54.71%
JunB
1e-446
15.90%
ETS
1e-106
3.18%
Mitotic
RUNX
1e-521
52.96%
JunB
1e-50
10.94%
TEAD2
1e-23
2.01%
G1
RUNX
1e-1566
59.01%
Fra1
1e-260
19.61%
ETS1
1e-51
4.32%
P-value
% of Targets

Figure 2

A. Interphase Prophase Prometaphase Metaphase Anaphase Telophase

RUNX1

UBF

DAPI

Merged

B.

Signal Overlay

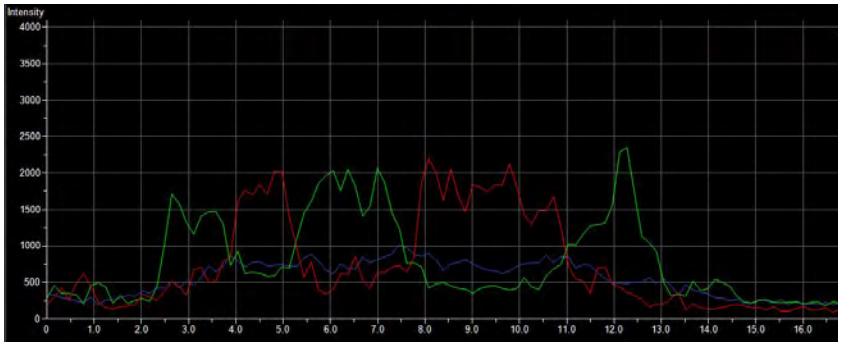

Interphase

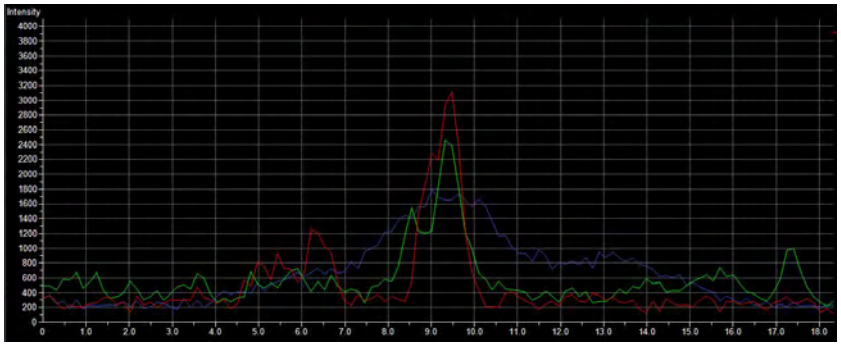

Metaphase

Figure 3

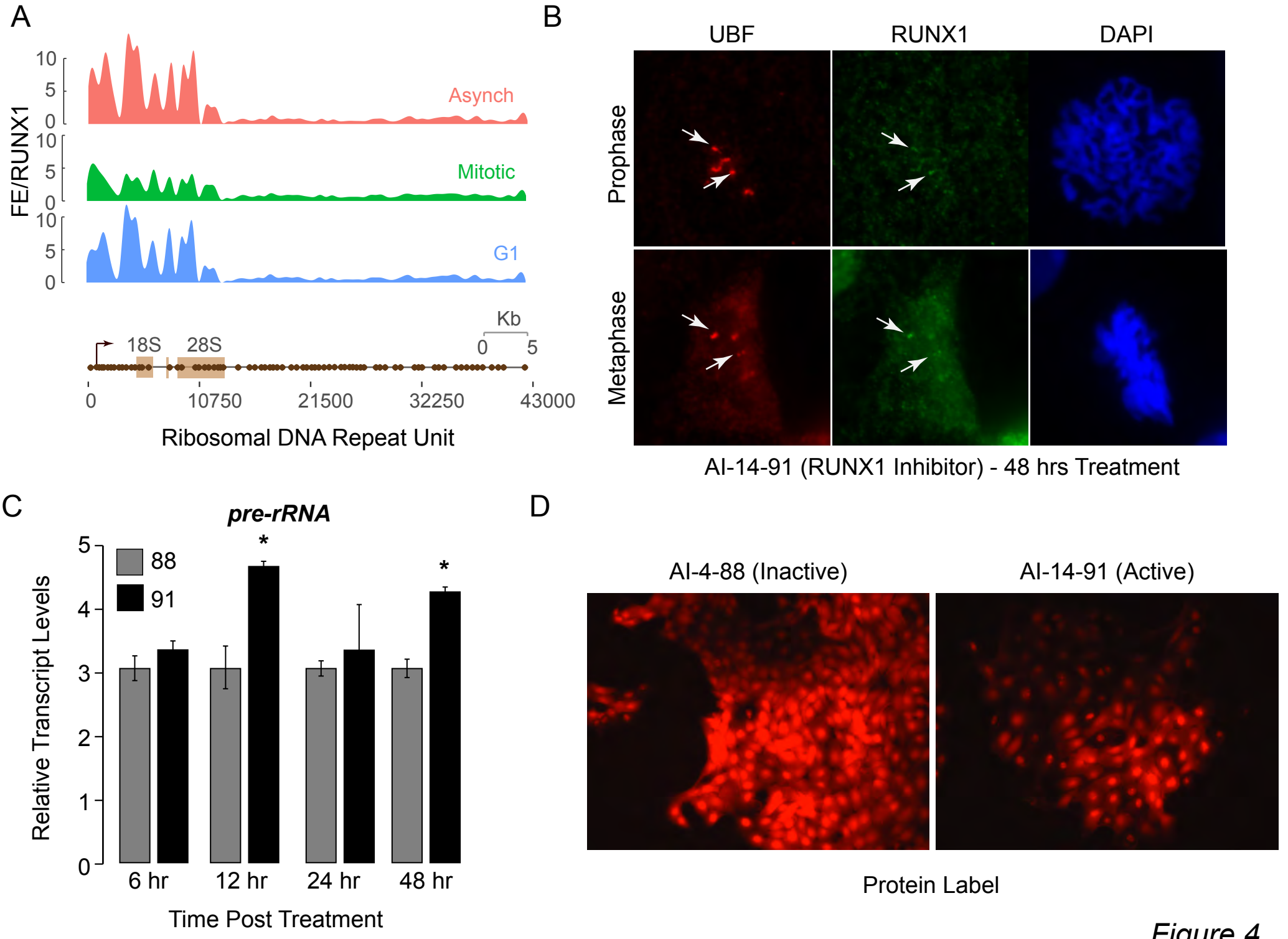
A
FE/RUNX1
10
5
0
Asynch
Mitotic
G1
Kb
18S
28S
0
5
0
10750
21500
32250
43000
Ribosomal DNA Repeat Unit
B
UBF
RUNX1
DAPI
Prophase
Metaphase
AI-14-91 (RUNX1 Inhibitor) - 48 hrs Treatment
C
pre-rRNA
88
91
*
*
Relative Transcript Levels
0
1
2
3
4
5
6 hr
12 hr
24 hr
48 hr
Time Post Treatment
D
AI-4-88 (Inactive)
AI-14-91 (Active)
Protein Label

Figure 4

A

Gene Set Name [# of Genes]	# of Bookmarked Genes
HALLMARK_ESTROGEN_RESPONSE_LATE [200]	12
HALLMARK_MTORC1_SIGNALING [200]	12
HALLMARK_TNFA_SIGNALING_VIA_NFKB [200]	12
HALLMARK_APICAL_JUNCTION [200]	11
HALLMARK_ESTROGEN_RESPONSE_EARLY [200]	10
HALLMARK_G2M_CHECKPOINT [200]	10
HALLMARK_P53_PATHWAY [200]	10
HALLMARK_DNA_REPAIR [150]	8
HALLMARK_E2F_TARGETS [200]	9
HALLMARK_NOTCH_SIGNALING [32]	4

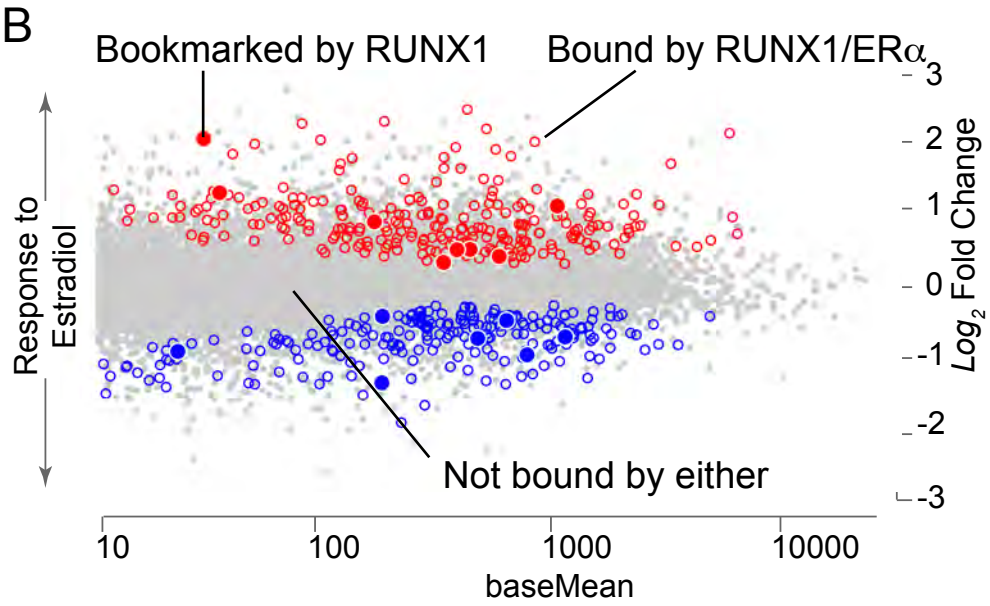

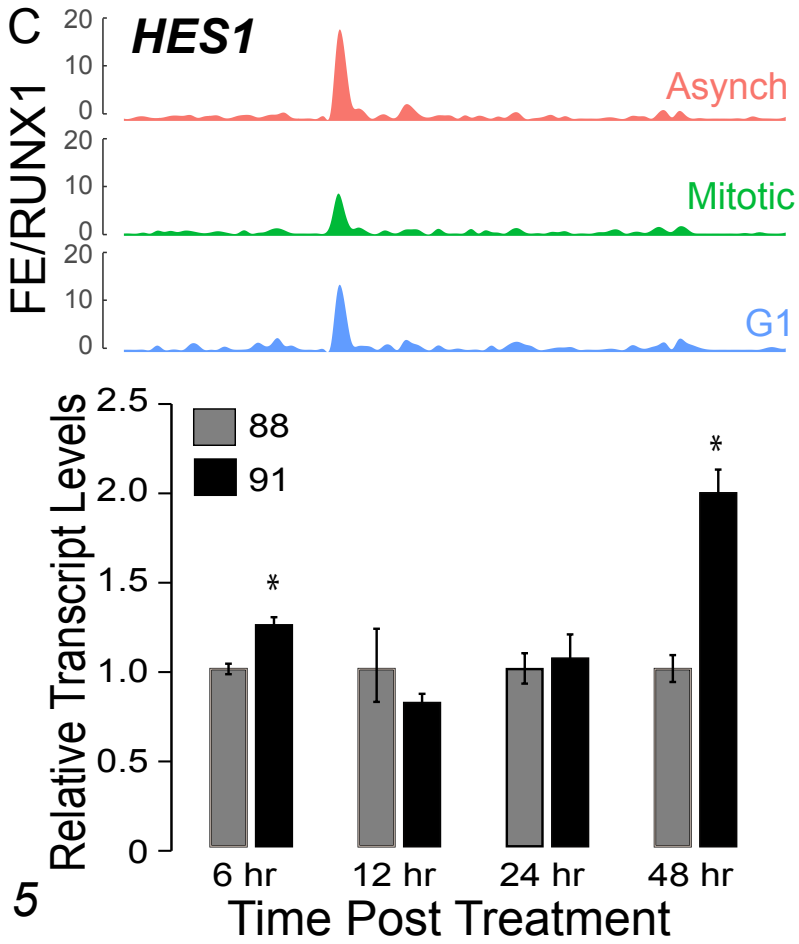

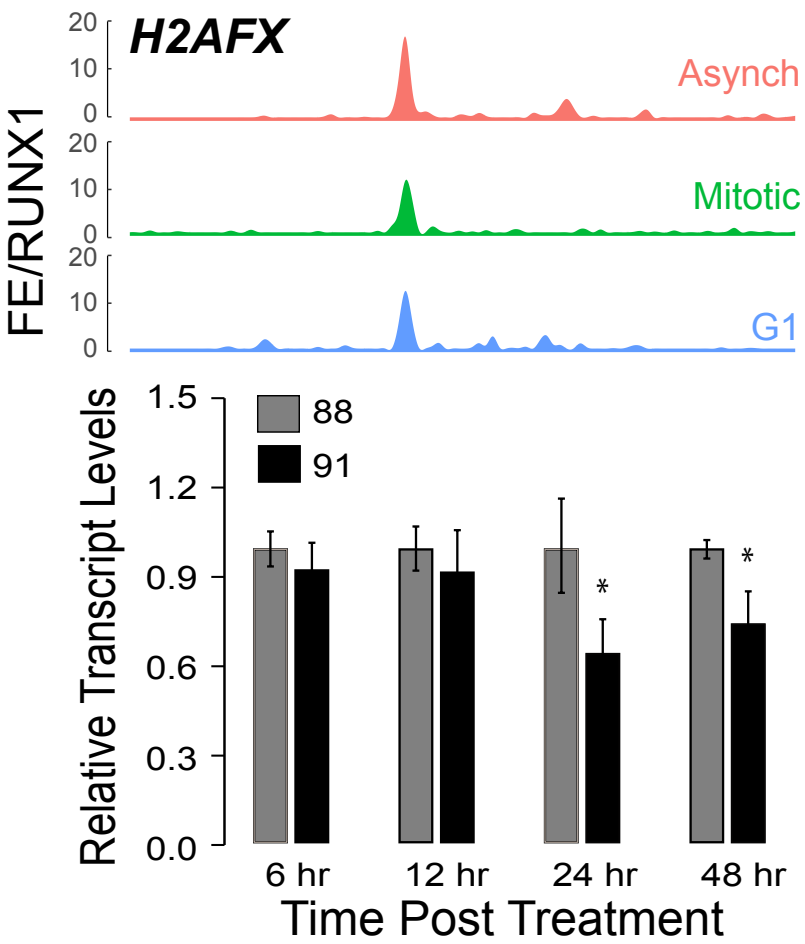

Figure 5

A.

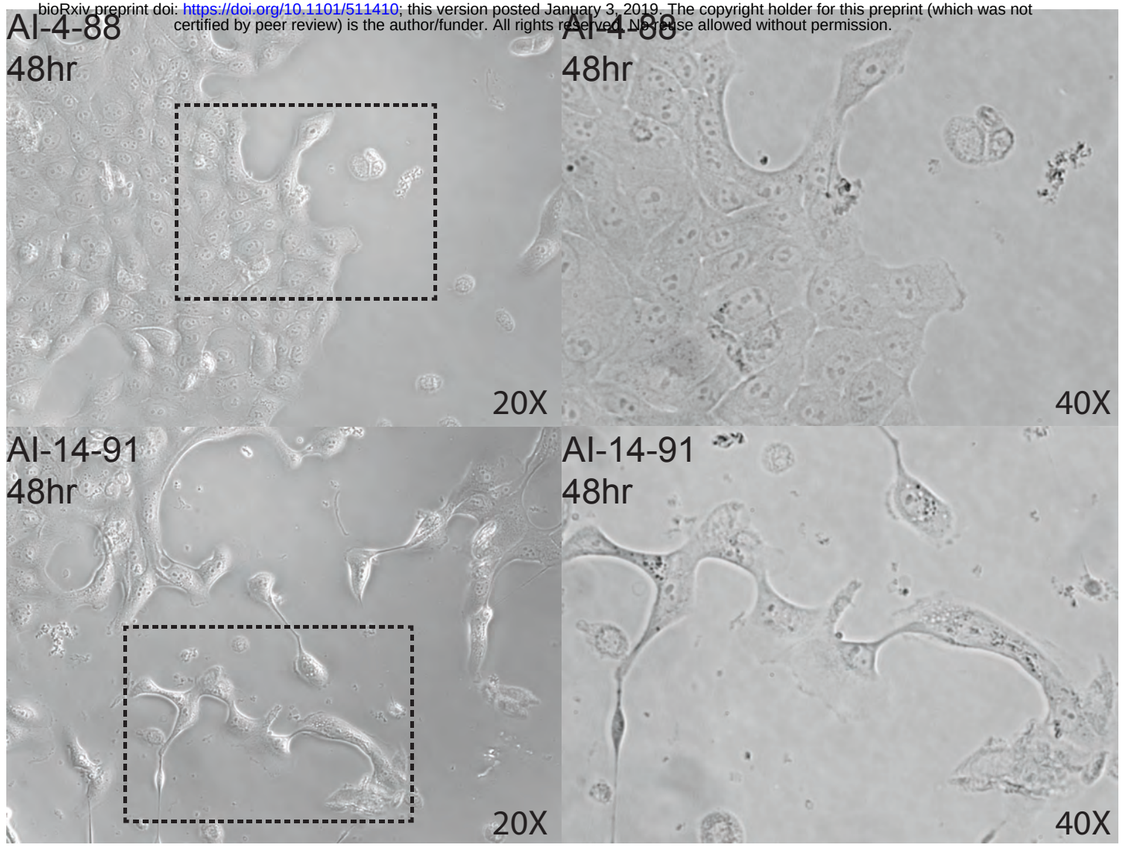

B.

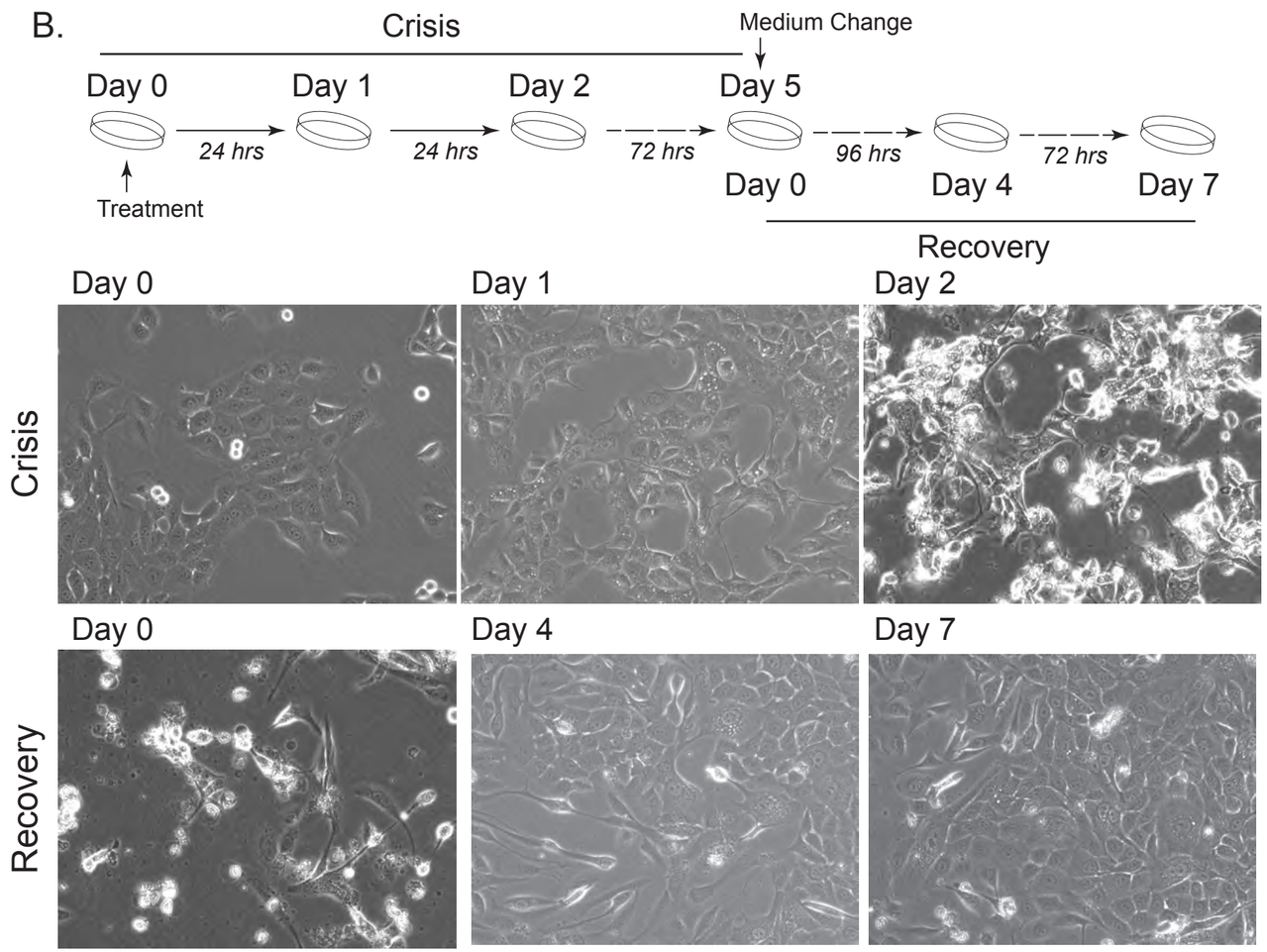

C.

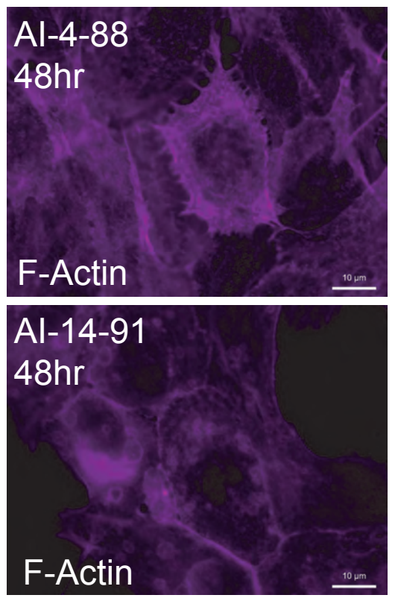

D.

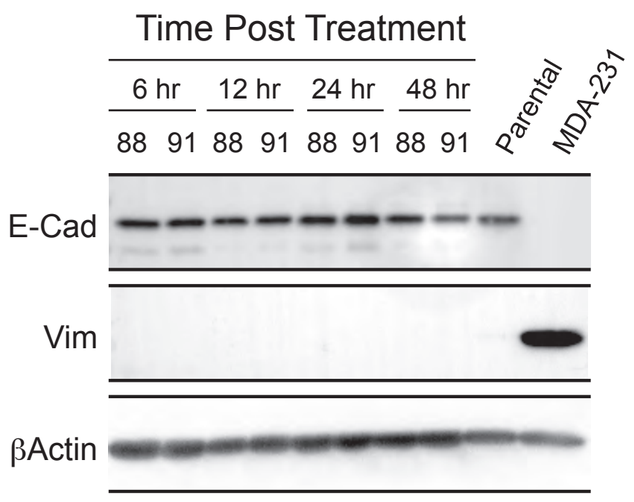

E.

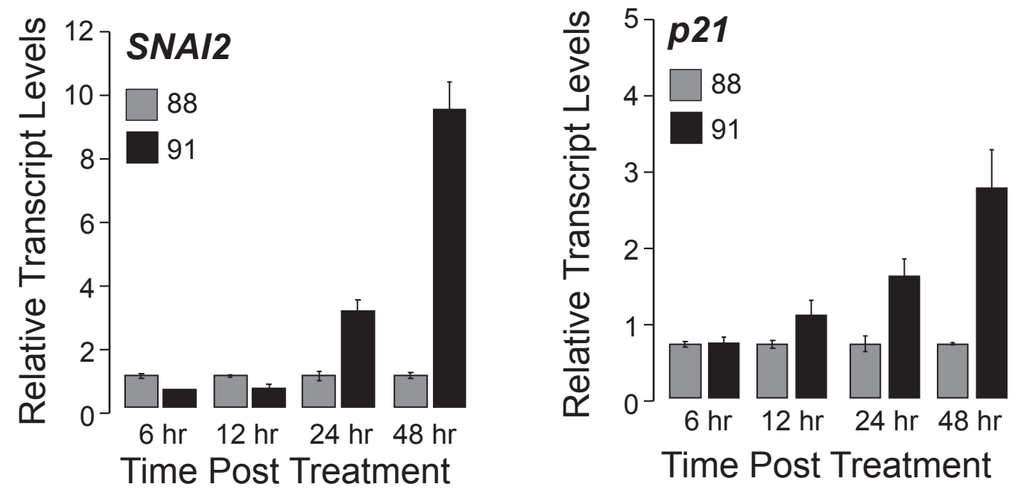

Figure 6